Orbital Debris
Quarterly News

Inside...

A publication of the
NASA Orbital Debris
Program Office (ODPO)

2021 UN COPUOS STSC Session

The 58th session of the Scientific and Technical Subcommittee (STSC) of the United Nations (UN) Committee on the Peaceful Uses of Outer Space (COPUOS) was held at the Vienna International Centre (VIC) in Vienna on 19-30 April 2021. It was postponed from the usual February schedule because of the COVID-19 pandemic. The session followed an in-person and virtual hybrid format, although most attendees participated remotely due to VIC on-site and travel restrictions.

During the Space Debris sessions, many delegates expressed their concerns for the worsening orbital debris problem. Many of them also emphasized the importance of and promoted the need for better global adoption and implementation of existing orbital debris mitigation best practices, including the Inter-Agency Space Debris Coordination Committee Space Debris Mitigation Guidelines, the UN COPUOS Space Debris Mitigation Guidelines, and the UN COPUOS Guidelines for the Long-Term Sustainability of Outer Space Activities (LTS). Several UN COPUOS Member States also provided technical presentations to highlight their recent orbital debris research activities. They included "Space Debris Research at JAXA," "U.S. Space Debris Environment and Activity Updates," "Space Debris/Sustainability Activities in ESA in 2020," "The German Experimental Space Surveillance and Tracking Radar - A high-performance experimental radar for space surveillance," and "2020 Space Debris Activities in France: Highlights." All technical presentations are available at the UN COPUOS STSC website (https://www.unoosa.org/oosa/en/ourwork/copuos/stsc/technical-presentations.html).

Informal meetings for the LTS Working Group also took place during the 58th STSC session. After several constructive consultations, the Working Group finally reached a consensus on the bureau for the next phase of the LTS activities (LTS 2.0). As a result, the Subcommittee elected R. Umamaheswaran from India as the Chair of the Working Group. It is expected that he will lead the LTS 2.0 activities starting at the 64th COPUOS session in late August. ♦

DAS 3.1 NOTICE

Attention DAS Users: DAS 3.1.1 has been updated to DAS 3.1.2. Previous versions of DAS should no longer be used. NASA regulations require that a Software Usage Agreement must be obtained to acquire DAS 3.1.2. DAS 3.1.2 requires the Windows operating system and has been extensively tested in Windows 10.

To begin the process, click on the Request Now! button in the NASA Software Catalog at https://software.nasa.gov/software/MSC-26690-1. Users who have already completed the software request process for earlier versions of DAS 3.x do not need to reapply for DAS 3.1.2. Simply go to your existing account on the NASA Software portal and download the latest installer.

An updated solar flux table (created 28 June 2021) can be downloaded for use with DAS 3.1.2.

PROJECT REVIEW

Comparison of the NASA ORDEM 3.1 and ESA MASTER–8 Models

A. MANIS, M. MATNEY, A. VAVRIN, D. GATES, J. SEAGO, AND P. ANZ-MEADOR

The NASA Orbital Debris Engineering Model (ORDEM) and ESA's Meteoroid and Space Debris Terrestrial Environment Reference (MASTER) model constitute the two premier orbital debris engineering models. The latest versions of these models – ORDEM 3.1 [1] and MASTER-8 [2] – were recently released, providing significant model improvements and representing their agency's best estimate of the current and near-future orbital debris environment.

Modeling the orbital debris environment is a complex process that relies on data for physical characteristics of space objects and debris generating events. Not all debris objects can be tracked due to their small size and/or complex orbits and limitations of available sensors used for detecting debris. In particular, objects approximately 1 mm in size are too small to be detected by ground-based sensors, yet millimeter-sized orbital debris drives mission-ending risk to robotic spacecraft in low Earth orbit (LEO). Models for the orbital debris environment are therefore necessary to assess the evolving orbital debris environment, and engineering models like ORDEM and MASTER allow for evaluation of the effects of this changing environment on planned space missions.

As these models are developed by independent processes and using different underlying datasets and assumptions, it is of interest to understand how the models compare. Differences between each model's results can shed light on aspects of orbital debris modeling that may not be well-understood or regions of space where insufficient data currently exists. Conversely, similarities in their results can indicate a sufficient fundamental understanding of the environment. This project review provides a summary comparison of fluxes produced by ORDEM 3.1 and MASTER-8; a more detailed comparison can be found in [3]. Similar comparisons have been performed for previous versions of these two models (ODQN, vol. 19, issue 2, April 2015, pp. 4-6). These studies provide an objective assessment on regions where the orbital debris environment is well-modeled, as well as regions where additional information may be needed.

Model Overview

ORDEM 3.1 and MASTER-8 both provide estimates of the orbital debris flux (number per m² per year) from LEO up to at least geosynchronous Earth orbit (GEO). Both models are based on the U.S. Space Surveillance Network (SSN) catalog, which provides coverage of objects down to approximately 10 cm in LEO and 1 m in GEO, and both include historical and statistically projected future breakup events. The models are tuned using available datasets from *in situ* and ground-based sensors. Additional details on development and validation of ORDEM 3.1 can be found in [4], and details on MASTER-8 are provided in [2].

One of the primary distinctions between the two models is in their underlying sub-populations. ORDEM 3.1 uses a breakdown by source type to build the underlying populations: intact objects (mission-related debris, spacecraft, and upper stages), fragmentation debris, degradation debris, and Sodium-Potassium (NaK) coolant droplets from the Radar Ocean Reconnaissance Satellite (RORSAT) class of spacecraft. However, as originally implemented in ORDEM 3.0 [5], the ORDEM 3.1 output flux includes a breakdown of debris into material density categories to better characterize the potential debris risk posed to upper stages and spacecraft. Five density categories are modeled, including intact objects; low-density (LD, 1.4 g/cm³) fragments; medium-density (MD, 2.8 g/cm³) fragments and degradation debris; high-density (HD, 7.9 g/cm³) fragments and degradation debris; and NaK droplets (0.9 g/cm³). Note while these material density categories represent a range of values, the specific values indicated here are those used for risk assessments.

MASTER-8 is an event-based simulation of all known events that generate debris, in addition to objects from the SSN catalog. "Source" models, so-called because they assign an origin to each individual object, are used to simulate the artificial objects and their orbital evolution. These sources, also used in the output flux breakdown, include explosion and collision fragments, launch- and mission-related objects, solid rocket motor (SRM) slag and dust, NaK droplets, paint flakes, ejecta, and multi-layer insulation (MLI) objects. MASTER-8 also includes a micrometeoroid component; however, for the comparisons considered here, that component has been excluded.

Simulation Cases and Results

Simulation cases for a Sun-synchronous orbit (SSO), nominal International Space Station (ISS) orbit, and geosynchronous transfer orbit (GTO) are shown in Table 1. These cases were chosen to include a broad spectrum of the modeled debris population. All simulations were performed for the year 2016, which is the first year of the future projection for ORDEM 3.1 and the most recent historic reference population for MASTER-8. All simulations assume a spherical target geometry, *i.e.,* the flux is integrated over all directions. Note that ORDEM 3.1 outputs cumulative fluxes for diameters from 10 μm to 1 m, while MASTER-8 outputs cumulative fluxes for diameters between 1 μm and 100 m.

The results for the SSO, ISS, and GTO cases are shown in Figures 1, 2, and 3, respectively. All cases show similar general behavior in the flux trends of ORDEM 3.1 and MASTER-8. At a diameter of 1 m, the flux results of each model are nearly equivalent, with MASTER-8 slightly

Table 1. Parameters for the simulation cases

Case	Semi-Major Axis (km)	Eccentricity	Inclination (°)	Argument of Perigee, ω (°)	Right Ascension of the Ascending Node, Ω (°)
SSO	7171	0.0001	98.0	0.0	0.0
ISS	6771	0.0001	51.6	0.0	0.0
GTO	24000	0.73	28.5	0.0	0.0

ORDEM 3.1/MASTER-8 Comparison
continued from page 2

higher than ORDEM 3.1 for the ISS case. At this size, most LEO objects are well-tracked, and very few additional simulated objects are introduced by either model, so similar results are expected. Below 1 m, ORDEM 3.1 has a slightly lower flux than MASTER-8, down to approximately 3 mm for the SSO case and approximately 2 mm for the ISS and GTO cases. For smaller sizes, the ORDEM 3.1 fluxes are consistently higher. At 1 mm, the ORDEM 3.1 flux is approximately 1.5 to 2 orders of magnitude higher than the MASTER-8 flux for all cases considered here. The models converge more near 100 μm, but the spread increases again for smaller sizes. ORDEM 3.1 is approximately 2 and 2.5 orders of magnitude higher than MASTER-8 at 10 μm for the SSO and ISS cases, respectively. For the GTO case, this difference is reduced to approximately 1 order of magnitude. Modeling the sub-millimeter diameter regime is complex and relies on sparse data at limited times/altitudes for model calibration; thus, the differences between the models are most pronounced for these smaller sizes.

The qualitative difference between the flux results for ORDEM 3.1 and MASTER-8 at sub-millimeter sizes can be attributed to the differences in how the model populations were developed. ORDEM 3.1 exhibits smooth logarithmic behavior throughout, with a steeper increase from a few millimeters down to 1 mm diameter. This steeper increase is a result of the transition between populations dominated by fragmentation debris, which are scaled using ground-based radar data, and degradation debris, which are fit to impact data from returned surfaces. The smooth logarithmic behavior is a result of the process to calculate cumulative fluxes at specific sizes. Eleven half-decade size thresholds, or fiducial points, are considered in calculating and presenting the cumulative fluxes: 10 μm, 31.6 μm, 100 μm, 316 μm, 1 mm, 3.16 mm, 1 cm, 3.16 cm, 10 cm, 31.6 cm, and 1 m. Fluxes at points between these are calculated by interpolation. The MASTER-8 fluxes generally show more dynamic behavior, particularly evident in the stair-step behavior seen in the ISS flux results at around 500 μm, 200 μm, and 10 μm. This is due to the superposition of individual sources (in this case paint flakes, SRM slag, and SRM dust), which have their own orbital dynamics due to the different area-to-mass ratio of individual objects. For a nominal ISS orbit at around 400 km altitude, atmospheric drag plays a major role in the evolution of the objects, which leads to different orbital decay behaviors of the different sources. Combined with individual release mechanisms for each source, this leads to the stair-step behavior shown.

In addition to comparing the fluxes for these simulation cases, Figure 4 presents a comparison using data collected from impacts to the Hubble Space Telescope (HST) Bay 5 MLI and Wide Field Planetary Camera (WFPC)-2 radiator, which were used for ORDEM 3.1 validation [3]. This dataset represents the most recent *in situ* data available at HST altitude. The comparison is presented against a total micrometeoroid plus orbital debris environment, utilizing the NASA Meteoroid Environment Model Release 2.0 (MEM R2) for the micrometeoroid component. The HST Bay 5 MLI and

WFPC-2 radiator surfaces had exposure times of 1990-2009 and 1993-2009, respectively; for the purposes of comparing the model fluxes to the data, the ORDEM 3.1 and MASTER-8 results presented in Figure 4 are averaged over the longer exposure time of the HST Bay 5 MLI. The MLI data presented is an average of two scenarios, assuming all impactors as either MD (nominal material density 2.8 g/cm³) or HD (nominal material density 7.9 g/cm³) in interpreting particle diameter from the impact feature size, because the MLI impacts are still undergoing chemical analyses to assess impactors as micrometeoroid or orbital debris. The limiting size of the MLI impactors is based on the transition zone from penetrations to craters. Note that the particle size interpretation for the MLI impacts is based on laboratory impact tests conducted using large
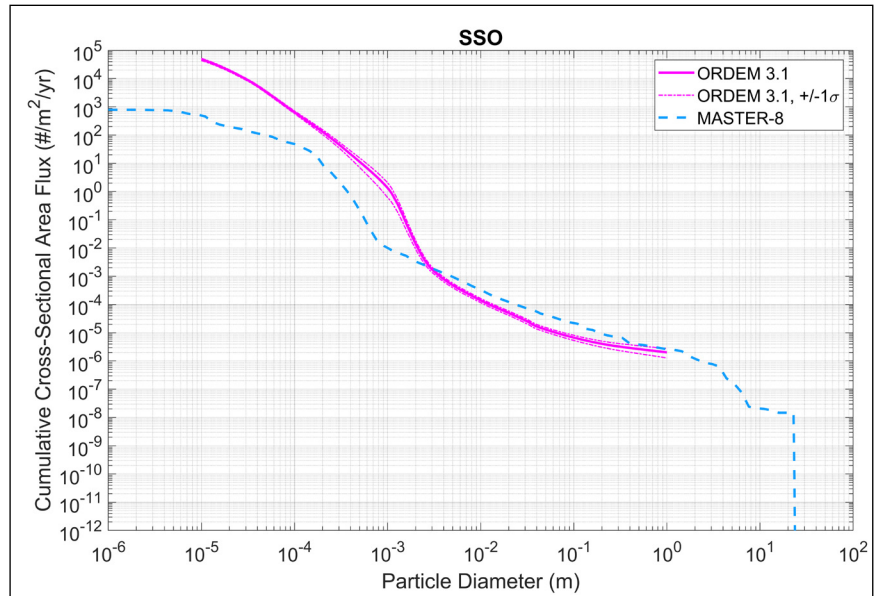

Figure 1. Cumulative total flux for a sun-synchronous orbit at 800 km altitude.
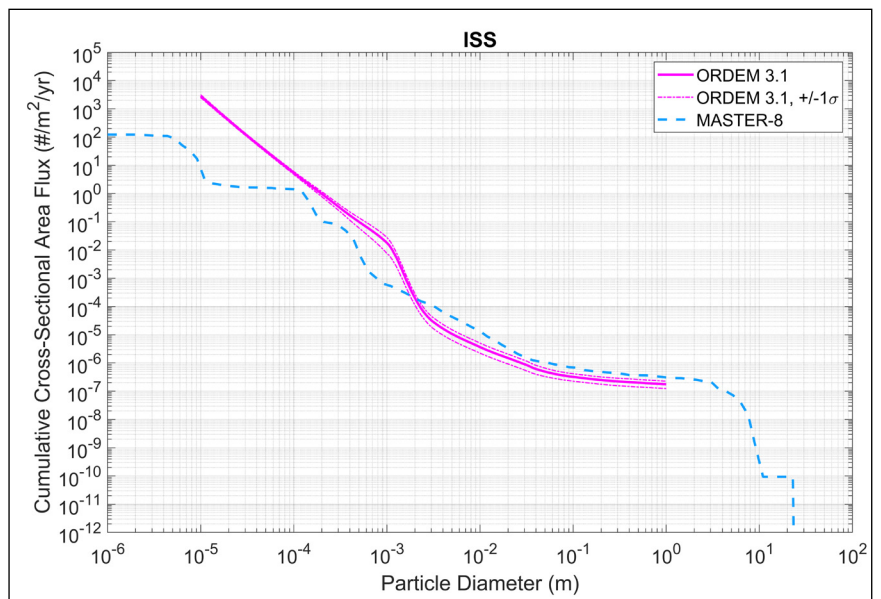

Figure 2. Cumulative total flux for a nominal ISS orbit.

ORDEM 3.1 / MASTER-8 Comparison

continued from page 3

particles (much greater than the MLI thickness), and the results were extended to all size impactors, with the assumption that the transition zone and penetration behavior is similar to that of aluminum plates. The error bars shown for the particle diameters cover the minimum to maximum of the individual MD and HD uncertainties. The WFPC-2 radiator impacts shown have been assessed as to impactor type, and those designated as orbital debris are included with their corresponding assigned material densities. ORDEM 3.1 and MASTER-8 both show very good agreement to the data where the data is most complete, at approximately 100–300 μm. As with the previous flux results, the difference between the models grows where the data is lacking, in particular near 1 mm. Near 1 mm, the MASTER-8 + MEM R2 curve is close to the MEM R2 curve, indicating that the MASTER-8 debris flux is lower than the modeled micrometeoroid flux for these sizes. In contrast, the ORDEM 3.1 debris flux is significantly higher at these sizes.

Figure 3. Cumulative total flux for a typical GTO with an apogee altitude of 35,149 km and a perigee altitude of 109 km.

Figure 4. Comparison of the cumulative cross-sectional area flux vs size between MASTER-8, ORDEM 3.1, and impact data from the HST Bay 5 MLI and WFPC-2 radiator. The MASTER and ORDEM curves include the meteoroid flux estimates from the MEM R2 model. The MLI data points represent an average from assuming all impactors as either MD or HD. The MEM R2 model results are also shown for reference.

Conclusions

The regions of similarities and differences between the ORDEM 3.1 and MASTER-8 models identify critical orbit and size regimes where there are currently insufficient measurements. The agreement between the models is best where there is high quality data on the orbital debris environment, as evidenced by the comparison of the models to the HST MLI and WFPC-2 impact data. There are clear differences in the flux estimates by the two models mainly in orbit and size regimes that are only poorly covered by underlying measurement data, particularly at SSO altitudes and in the critical millimeter-size range, which drives mission-ending risk to robotic spacecraft in LEO. The comparisons presented here create incentives to collect measurement data in these target orbits and size regimes to increase the fidelity of both models. Orbital debris is a global issue, so collaborative international studies, as summarized here, will continue to improve our understanding of the orbital debris environment.
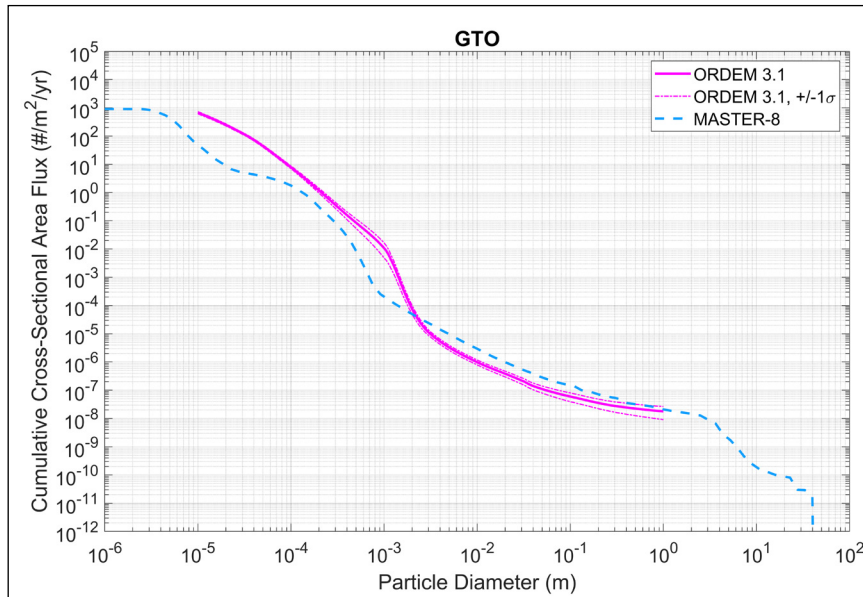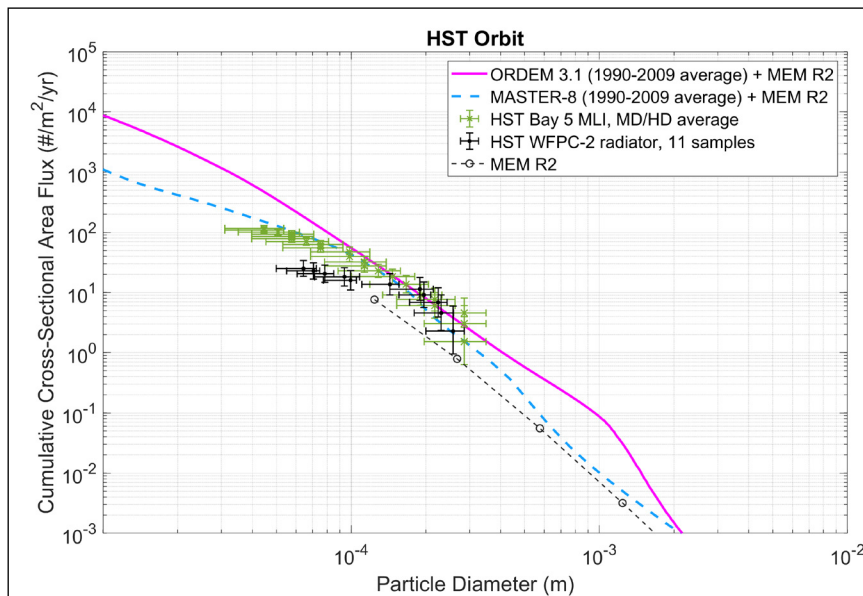
References

1. Vavrin, A., *et al.*, "NASA Orbital Debris Engineering Model ORDEM 3.1 – Software User Guide," NASA/TP-2019-220448, NASA Johnson Space Center, Houston, TX, USA, (2019).

2. Horstmann, A., *et al.*, "Enhancement of S/C Fragmentation and Environment Evolution Models," ESA contract No. 4000115973/15/D/SR, (2020).

3. Horstmann, A., *et al.*, "Flux comparison of MASTER-8 and ORDEM 3.1 modelled space debris population," in 8th European Conference on Space Debris, 20 April 2021 - 23 April 2021, Darmstadt, Germany, published by ESA Space Debris Office, (2021).

4. Matney, M., *et al.* "The NASA Orbital Debris Engineering Model 3.1: Development, Verification, and Validation," Paper presented at the 1st International Orbital Debris Conference, Sugar Land, TX, 9-12 December 2019.

5. Krisko, P.H., "The New NASA Orbital Debris Engineering Model ORDEM 3.0," AIAA 2014-4227, (2014). ♦

PROJECT REVIEW

Validation of a New Fiber-Reinforced Polymer Charring Model with X-Ray Computed Tomography

B.R. GREENE AND C. L.OSTROM

Modeling the destructive reentry of space vehicles is critical to estimating the human casualty risk posed by fragments that may survive to impact Earth's surface. Several recent studies have made clear that the current standard assumptions for how fiber-reinforced polymer (FRP) composites demise are inadequate for the task of computing ground casualty risk. An initial study by Lips, *et al.*, determined from arc-jet tests that carbon-overwrapped pressure vessels may not demise even when most of the polymer matrix has pyrolyzed [1]. The NASA Orbital Debris Program Office (ODPO) followed up on these studies with the Phase I and Phase II test campaigns conducted at the University of Texas at Austin (UT) Inductively Coupled Plasma (ICP) Torch Facility, described in detail in references [2] and [3], respectively.

The large number of material samples tested during these campaigns has provided a solid base of real-world data against which to compare new composite char models currently being developed. In addition, the ODPO has incorporated X-ray Computed Tomography (CT) imaging as a novel, non-destructive method for determining the extent of char in samples of FRP materials. This new method of measuring the extent of char formation in test coupons allows direct measurement of the exact percentage of charred material instead of inferring from volume change and mass loss. These data were then used to validate a charring model that is in development for inclusion in the ODPO's Object Reentry Survival Analysis Tool (ORSAT) 7.

Measurements of Char Rate and Extent

The char rate tests were performed at UT's ICP Torch Facility, a 50 kW air and argon plasma generator capable of applying a cold wall heat flux of up to 240 W/cm² with an air plasma [4]. The current study required the oxidation environment to approximate that at a 60+ km altitude, where most of the thermal ablation of the satellite occurs. Since the ICP facility operates at atmospheric pressure, this oxidation level was achieved by running the torch on a 98% argon and 2% air mixture. This had the side effect of greatly reducing the maximum heat flux of the facility to approximately 35 W/cm², and a maximum sustainable heat flux (without stressing the system) of approximately 30 W/cm². Each material sample was therefore tested at both a "low" cold wall heat flux of 18 W/cm² to 20 W/cm² and a "high" cold wall heat flux of 28 W/cm² to 30 W/cm², as measured by a Gardon gauge with a similar shape and size to the sample coupons before and after each test. Both a pure argon atmosphere and the 98/2 mix mentioned above were used to cover as much of the parameter space as possible with the facility.

For the char rate tests in this article, three different sample materials were investigated: a carbon fiber-reinforced epoxy resin, a carbon fiber-reinforced cyanate ester resin, and a glass fiber-reinforced polyester resin (G10). The carbon fiber/epoxy and G10 were both commercial off-the-shelf products, while the carbon fiber/cyanate ester was acquired from off-cuts of custom layups for flight hardware produced at the NASA Johnson Space Center (JSC). These three materials were chosen as representative of a broad range of FRP composites used in spacecraft.

As mentioned in [3], to maximize the speed at which test samples could be exchanged between tests, a rectangular prism shape was chosen for all test coupons. This greatly simplified the test apparatus and procedure. However, the complexity of the flow field and 3D nature of the heat flux made it impossible to assume a 1D propagation of the pyrolysis front and made inferring the char extent within the sample from the mass loss alone much more difficult.

Utilizing research from JAXA and NASA Ames, which used X-ray CT scans to investigate the post-flight thermal protection systems of the Hayabusa reentry capsule [5] and the Stardust reentry capsule [6], a method was devised of directly measuring the char extent inside the test sample coupons and using these measurements to calculate the average char density.

Using a Nikon XTH 320 X-ray CT scanning machine in the Astromaterials X-ray Computed Tomography Laboratory at JSC, 27 test samples were scanned. Figure 1 shows a sample cross section image from both a carbon fiber-reinforced epoxy sample and a glass fiber-reinforced polyester sample. In the image, the charred region on the top of the sample is clearly demarcated from the uncharred region by both a change in X-ray transmissivity of the fiber bundles themselves as well as an increase in the void space between the fibers where the resin has pyrolyzed.

This change in X-ray transmissivity allows the charred and uncharred regions of the scan to be isolated using a simple threshold filter algorithm. Once the regions have been identified, a minimum containing surface can be found for the region and used to calculate the exact char
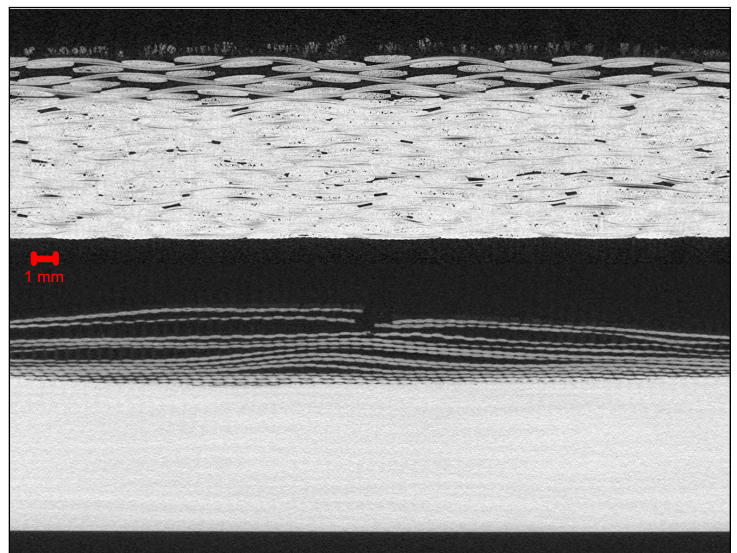
Figure 1. X-ray CT Scan cross section of carbon fiber-reinforced epoxy resin (top) and G-10 glass fiber-reinforced polyester resin (bottom) exposed to 20 W/cm² of plasma heat flux for 40 seconds.

ORSAT Model Improvements

continued from page 5

volume, virgin material volume, and total test coupon volume for each charred sample. Finally, using the mass loss and the known density of the virgin material, an average char density can also be computed using Eq 1,

$$\rho_c = \frac{m_f - \rho_v V_v}{V_c} \qquad (1)$$

where ρ_c is the average char density, m_f is the final mass of the sample after testing, ρ_v is the density of the virgin material, V_v is the volume of the virgin material, and V_c is the char volume. The value of char volume and char density for each type of material scanned are shown in Figures 2 and 3, respectively. As expected, the char volume increases relatively linearly over the course of exposure to the plasma torch, though the rate slows down for G10 after 40 seconds and increases for carbon fiber/ epoxy after 40 seconds by approximately the same factor. For all of the materials, the char density shown in Figure 3 approaches a constant value of approximately 1 g/cc, which is consistent with the formation of a thin pyrolysis zone separating a volume of virgin material and a volume of completely charred material with only a small amount of the original matrix mass and most or all of the fiber mass remaining.

From the images in Figure 1, it can be concluded that this trend in the G10 is due to rapid delamination in the G10 followed by melting and ablation of the fiber bundles. The opposite trend in the carbon fiber/ epoxy is due to an initial lack of delamination to increase the char volume beyond that achieved through motion of the pyrolysis front. The linear nature of the increase in char volume for the carbon fiber/cyanate ester is explained by a complete lack of delamination of the woven fiber layers.

FRP Char Model

To better capture this charring behavior in ORSAT, the ODPO is developing a new model for FRP demise to be implemented in ORSAT 7, based on the model proposed by Hidalgo, *et al.* in [7]. This model has several advantages that make it preferable for use in ORSAT over others that incorporate chemical kinetics for oxidation and pyrolysis. The first is that implementing it requires very few changes to the underlying code structure of ORSAT, making errors less likely and resulting in a faster verification and validation process. Second, the model is relatively simple and will not negatively impact the computation time of a given ORSAT run. Finally, tailoring the model to any specific FRP material and layup requires only the results of a thermogravimetric analysis (TGA) of the material, a test that is both widely available and inexpensive. This makes it easy to provide accurate results even for proprietary materials that do not exist in the ORSAT material properties database.

To model the charring process, the problem is assumed to be separable into a thermal transport problem and a mass loss problem. The thermal transport problem is solved using a standard finite-difference approach assuming an inert material. The mass loss is calculated purely as a function of the temperature in any given mesh cell at the current time step, with a check to make sure the mass loss cannot go negative when the material cools.

A simple mass loss function can be constructed as a lookup table or curve fit from the mass vs. temperature curve obtained from TGA. Such a curve fit was calculated for G10 and the carbon fiber/epoxy using TGA performed by the Thermal Analysis Branch at JSC on behalf of the ODPO.

Finite difference model simulations were run for the G10 and carbon fiber/epoxy materials, emulating the char depth tests. Four fiducial points were used for each material to assess the progression of the char during a test. The char depth of the test sample used for comparison at each fiducial point was calculated using the average position of the pyrolysis zone within 5 mm of the center of the sample, the approximate location of the stagnation point of the plasma flow. The char depth is reported as the depth relative to the original height of the sample to eliminate any ambiguity from variation in the expansion of the char.
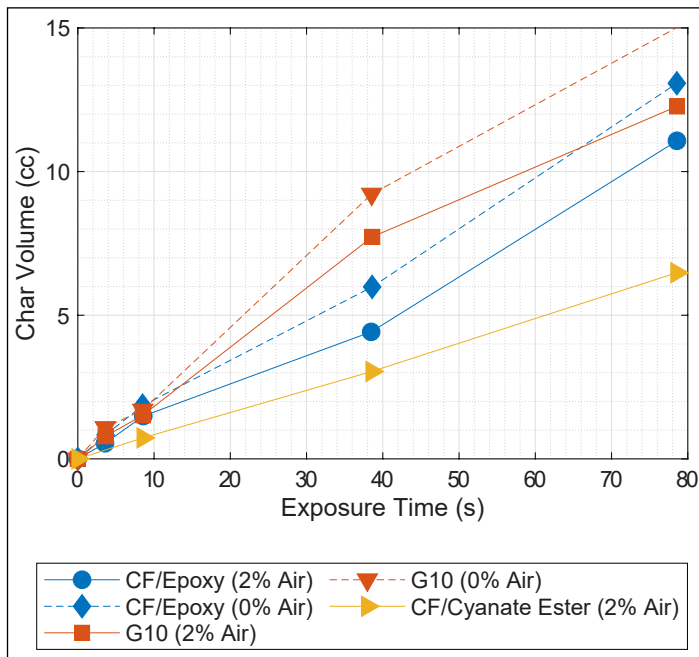
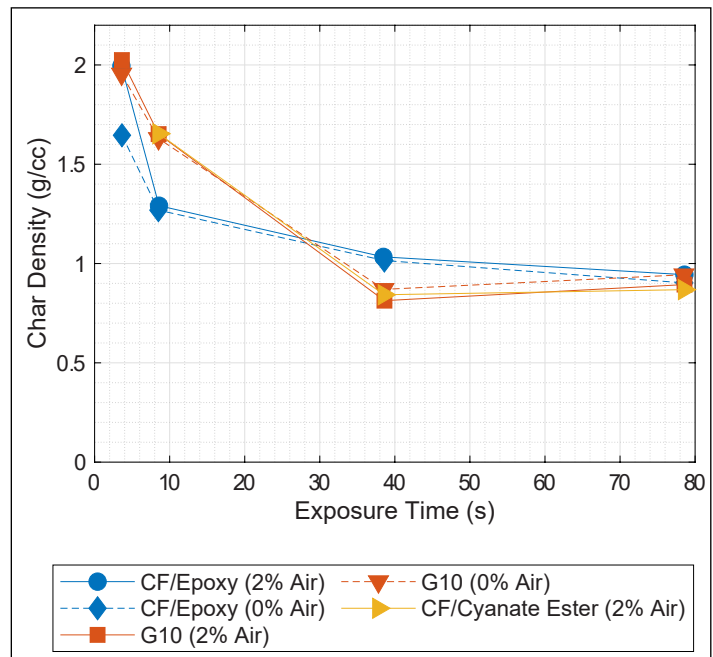*Figure 2. Char volume over exposure time for various FRP materials.*

Figure 3. Char density over exposure time for various FRP materials.

ORSAT Model Improvements

Table 1. Comparison of measured char depth with simulated char depth at each fiducial point for both G10 and carbon fiber/epoxy

	Time (s)	D_{char} (mm)	Simulated D_{char} (mm)	δ (mm)	δ (%)
G10	3.6	0.48	0.41	-0.07	-15
	8.5	0.80	1.00	0.20	25
	38.5	2.70	3.10	0.40	15
	78.5	5.40	5.10	-0.30	-6
Carbon Fiber/Epoxy	3.6	0.61	0.20	-0.41	-70
	8.5	0.92	1.00	0.08	7
	38.6	3.10	3.40	0.30	10
	78.6	6.20	5.90	-0.30	-5

The simulated char depth for G10 is determined as the location where the mass fraction decreases to 70% of the pristine material and the simulated char depth for carbon fiber/epoxy is determined as the location where the mass fraction decreases to 75% of the pristine material. These locations are based on the point at which the mass fraction in the TGA data started to asymptotically approach a constant value. Both simulations delivered comparable results and compared well with the char depth progression measured in the plasma torch test samples. A comparison of the model values with the test results at each fiducial point is shown in Table 1. Figure 4 shows the progression of the pyrolysis front over time compared with discrete data points from each test for both carbon fiber/epoxy and G10. While not all the data points match the simulation within the error bars of the char measurements, the simulation is generally within about 10% to 15% of the measured points. Some of the discrepancy likely is explained by the existence of delamination (and hence expansion) of the charred region, which the model assumes does not happen.

Conclusions

The ODPO is developing a new model for the reentry demise of fiber-reinforced plastic materials based on data obtained in the Phase I and Phase II Reentry Survivability Test Campaign. To validate the new model, the char extent inside 27 test coupons was measured using a novel X-ray CT approach. It is clear from Table 1 and Figure 4 that the model provides a reasonably accurate approximation of the pyrolysis front progression within both materials over the full range of exposure times tested.

Further work remaining on this project includes implementing the model in FORTRAN and optimizing computation time. Following that, further TGA tests need to be done to refine the mass loss models and specific heat capacity coefficients for the materials of interest. These improvements to FRP modeling in ORSAT 7 will enable more accurate reentry risk analysis of modern spacecraft and upper stages.

References
1. T. Lips, et al., "About the Demisability of Propellant Tanks During Atmospheric Re-Entry from LEO," in 8th International Association for the Advancement of Space Safety Conference, Melbourne, FL, 2016.

2. B. R. Greene, et al., "Demisability of GFRP and CFRP Components of Reentering Orbital Debris: Phase I Test Results," in 10th International Association for the Advancement of Space Safety Conference, El Segundo, CA, 2019.
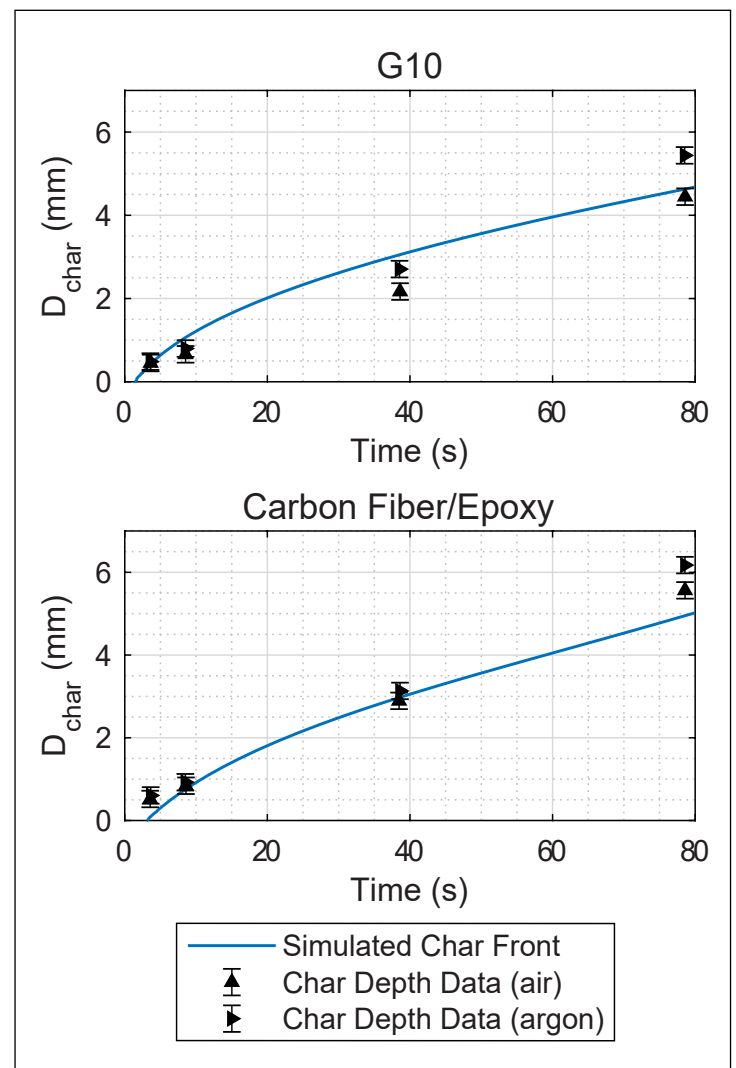

Figure 4. Comparison of simulated char progression in G10 (top) and carbon fiber/epoxy (bottom) with measured char depth at different exposure times.

ORSAT Model Improvements

3.   B. R. Greene, *et al.*, "Pyrolysis Rate and Yield Strength Reduction in Carbon Fiber and Glass Fiber Composites Under Reentry Heating Conditions," in 8th European Conference on Space Debris, Darmstadt, Germany, 2021.

4.   B. R. Greene, *et al.*, "Characterization of a 50 kW Inductively Coupled Plasma Torch for Testing of Ablative Thermal Protection Materials," in AIAA SciTech Forum - 55th AIAA Aerospace Sciences Meeting, Grapevine, TX, 2017.

5.   T. Suzuki, *et al.*, "Postflight Thermal Protection System Analysis of Hayabusa Reentry Capsule," Journal of Spacecraft and Rockets, vol. 51, no. 1, pp. 96-105, 2014.

6.   D. M. Empey, *et al.*, "X-Ray Computed Tomographic Investigation of Thermal Protection System Materials," in 50th AIAA Aerospace Sciences Meeting including the New Horizons Forum and Aerospace Exposition, Nashville, TN, 2012.

7.   J. P. Hidalgo, *et al.*, "A Framework for Evaluating the Thermal Behavior of Carbon Fibre Composite Materials," in Proceedings of the 2nd IAFSS European Symposium of Fire Safety Science, Nicosia, Cyprus, 2015. ♦

MEETING REPORTS

8th European Conference on Space Debris, 20-23 April 2021 (Virtual)

The 8th European Conference on Space Debris, hosted by the European Space Agency (ESA) Space Debris Office, was held virtually 20-23 April 2021. This latest edition of the quadrennial conference was a forum for information exchange, technical discussions, and networking between researchers, engineers, and decision makers from academia, government, and industry alike. The full program can be accessed via the link https://space-debris-conference.sdo.esoc.esa.int/page/programme

The four-day conference comprised 28 sessions, covering topics such as: Active and passive optical measurements; Debris mitigation techniques and processes; Radar measurements and attitude measurements; Hypervelocity impacts, protection and shielding; On-orbit and reentry risk assessments; Active removal, servicing, and remediation concepts; Re-entry modelling [sic] and tools; Orbit prediction, determination, and cataloging; Space situational awareness systems and applications; environmental impact assessments; Debris aspects of large constellations; AI (artificial intelligence) and ML (machine learning) for collision avoidance and services; Regulatory aspects, standardization, policies; Operational collision avoidance and services and novel concepts; and Future missions.

Representatives from the NASA Orbital Debris Program Office (ODPO) co-chaired four of these sessions and presented five papers, including: a description of the responsibilities of CubeSat operators under the updated US Government Orbital Debris Mitigation Standard Practices; a summary of the Haystack Ultrawideband Satellite Imaging Radar (HUSIR) 2019 observations; the application of X-ray imagery to the DebriSat project; a comparison of the latest Orbital Debris Engineering Model (ORDEM 3.1) and ESA's Meteoroid and Space Debris Terrestrial Environment Reference (MASTER-8); and a new analysis of the pyrolysis and strength of fiber-reinforced composite materials under reentry heating.

Each day of the conference also featured a panel discussion; Day 1's panel "The right attitude" covered the challenges and opportunities associated with determining attitude motion of debris objects in orbit. The panel on Day 2, "Time to act", discussed developments in debris mitigation technology and active debris removal; the panel on Day 3, "Leave no traces", focused on space sustainability, space as a global commons, and mitigation guidelines; the final panel on Day 4, "Be the first to move", covered space operations in a densely-populated orbital environment and automatic collision avoidance.

Papers and posters from the conference can be accessed from the conference proceedings database at https://conference.sdo.esoc.esa.int/proceedings/list.   ♦

The Spacecraft Anomalies and Failures (SCAF) Workshop, 11-12 May 2021 (Virtual)

The annual two-day Space Systems Anomalies and Failures (SCAF) Workshop was held virtually on 11-12 May 2021. The NASA Engineering and Safety Center hosted the unclassified Day 1 sessions and the National Reconnaissance Office hosted the Day 2 classified sessions. There were 146 attendees and 10 presentations for Day 1. Attendees and presenters included representatives from academia, industry, civil, and military space organizations. The theme this year was "Integrating Ground and Flight Anomalies", in an attempt to broaden the scope of the workshop.

The original "Spacecraft Anomalies and Failures" workshop name was changed this year to "Space Systems Anomalies and Failures" to broaden the scope of the event by adding the ground and launch system elements to the spacecraft bus and instrumentation systems that are critical to the overall success of a space program. For now, the organizers have retained the SCAF acronym to maintain the context with the long history of successful SCAF workshops.

A member from the NASA Orbital Debris Program Office provided the introductory presentation at the workshop on Day 1, discussing how many complex systems (not just those related to space activities) tend to suffer from the same sorts of anomalies and failures, including cascading failures and human factors. Highlights from the unclassified presentations included a wide range of topics including orbital breakup and debris generation, space environments and their effects on space systems, use of spacecraft telemetry for anomaly identification and attribution, tools and techniques to find root causes of anomalies, and commercial techniques for an integrated anomaly resolution process. The two-day workshop provided lively discussions among a wide range of community participants focusing on refining best practices for anomaly root cause attribution with an emphasis on practical case studies.   ♦

UPCOMING MEETINGS

These events could be canceled or rescheduled due to the COVID-19 pandemic. All information is current at the time of publication. Please consult the respective websites for updated schedule changes.

14-17 September 2021: 22nd Advanced Maui Optical and Space Surveillance Technologies Conference, Maui, Hawaii, USA (Hybrid)

The technical program of the 22nd Advanced Maui Optical and Space Surveillance Technologies Conference (AMOS) will focus on subjects that are mission critical to Space Situational Awareness/Space Domain Awareness. The technical sessions include papers and posters on Orbital Debris, Space Situational/Space Domain Awareness, Adaptive Optics & Imaging, Astrodynamics, Non-resolved Object Characterization, and related topics. The abstract submission deadline has passed. Additional information about the conference is available at https://amostech.com.

19-21 October 2021: 11th International Association for the Advancement of Space Safety (IAASS) Conference, Rotterdam, the Netherlands (Hybrid)

The 11th conference of the IAASS, organized in concert with the Japan Aerospace Exploration Agency, has as its theme "Managing Risk in Space." Major debris-related topics include designing safety into space vehicles, space debris mitigation and remediation, re-entry safety, nuclear safety for space missions, safety risk management and probabilistic risk assessment, and launch and in-orbit collision risk. The conference's abstract submission deadline has passed. Additional information for the 2021 IAASS is available at http://iaassconference2021.space-safety.org/ .

25-29 October 2021: 72nd International Astronautical Congress (IAC) – Dubai, United Arab Emirates

The IAC will convene with a theme of "Inspire, Innovate & Discover, for the Benefit of Humankind." The IAC's 19th IAA Symposium on Space Debris shall cover debris measurements, modeling, risk assessment including re-entry hazards, mitigation and remediation, hypervelocity impact and protection, political and legal aspects of space debris mitigation and removal, and allied subjects. The abstract submission deadline has passed. Additional information for the 2021 IAC is available at https://www.iafastro.org/events/iac/iac-2021/ and https://iac2021.org/ .

1-5 November 2021: Applied Space Environments Conference 2021 (Virtual)

The 2021 Applied Space Environments Conference, sponsored by NASA, NASA Jet Propulsion Laboratory, the Universities Space Research Association, and the National Science Foundation, is a forum for the space environment engineering and applied space science community to discuss the discipline's ability to support current space programs and to identify gaps in knowledge and technology needs required to meet future crewed and robotic exploration goals. Applicable environments and effects include micrometeoroid and orbital debris environments and hypervelocity impact effects on hardware. The abstract deadline closes 20 September 2021. Additional information about this free conference is available at https://www.nasa.gov/nase/conferences/ASEC

26 February-4 March 2022: 33rd International Symposium on Space Technology and Science, Beppu, Ōita Prefecture, Japan

The 33rd International Symposium on Space Technology and Science (ISTS) will be conducted jointly with the 10th Nano-Satellite Symposium & 14th International Academy of Astronautics (IAA) Low-Cost Planetary Missions Conference. ISTS will feature a dedicated session on Space Environment and Debris, including modeling, measurements, mitigation and protection, remediation, international cooperation, space weather, space situational awareness, space traffic management, and associated topics. The abstract submission deadline has passed. Additional information about the conference is available at https://www.ists.or.jp/.

28-30 March 2022: 3rd IAA Conference on Space Situational Awareness, Madrid, Spain

The International Academy of Astronautics (IAA) and the University of Florida will convene the 3rd IAA Conference on Space Situational Awareness in 2022; the University of Florida will provide a remote participation option should the COVID-19 pandemic not be resolved by meeting time. Topics include, but are not limited to, resident space object sensing, identification, association, risk assessment, remediation and reentry, and policy. Abstract submission closes on 15 December 2021. Please see http://reg.conferences.dce.ufl.edu/ICSSA/1575 or https://iaaspace.org/event/3rd-iaa-conference-on-space-situational-awareness-icssa-2021/ for further information.

26-28 April 2022: 2022 Cubesat Developer's Workshop, San Luis Obispo, CA, USA

This annual workshop will reconvene in April 2022, after having conducted the 2021 workshop virtually. Workshop format has not been revealed as the ODQN goes to press. Please see the workshop website https://www.cubesatdw.org/ for workshop details as they develop.

Monthly Effective Number of Objects in Earth Orbit
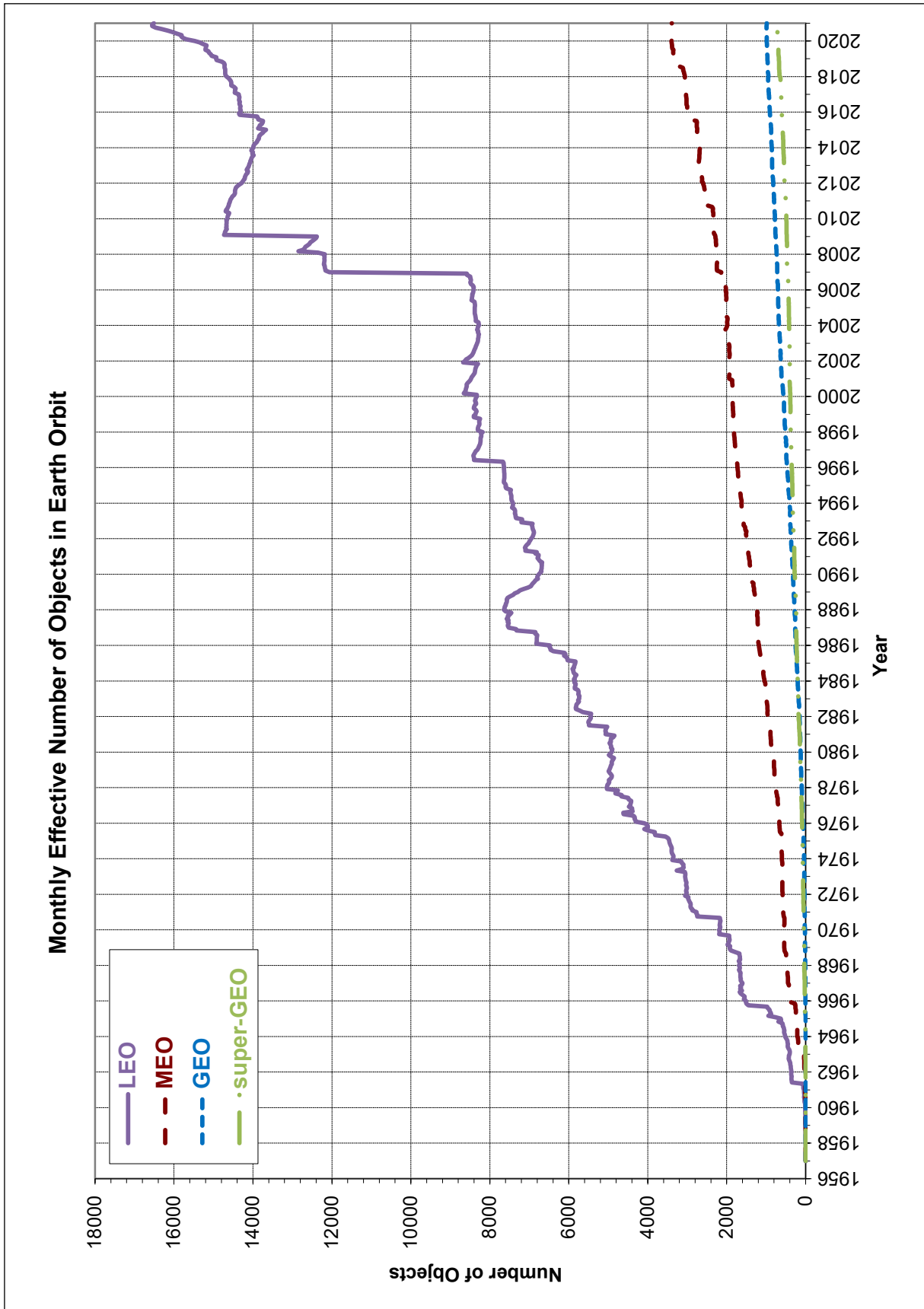
Monthly Effective Number of Cataloged Objects in Earth Orbit by Orbital Regime cataloged by the U.S. Space Surveillance Network (SSN), except those with SSN numbers of 80,000 and greater. This chart displays a summary of all objects in Earth orbit officially cataloged by the U.S. Space Surveillance Network. Low Earth orbit (LEO) includes resident space objects (RSOs) with altitudes within or crossing below 2,000 km; middle Earth orbit (MEO) RSOs with altitudes within or crossing the range from 2,000 km to 35,586 km; geosynchronous orbit (GEO) RSOs with altitudes within or crossing the range from 35,586 km to 35,986 km; and the remainder with altitudes within or crossing the range from 35,986 km to 600,000 km. "Effective" number sums the fraction of each orbit that falls within the specified ranges. Cataloged objects without available orbital elements are excluded.

Monthly Effective Mass of Objects in Earth Orbit
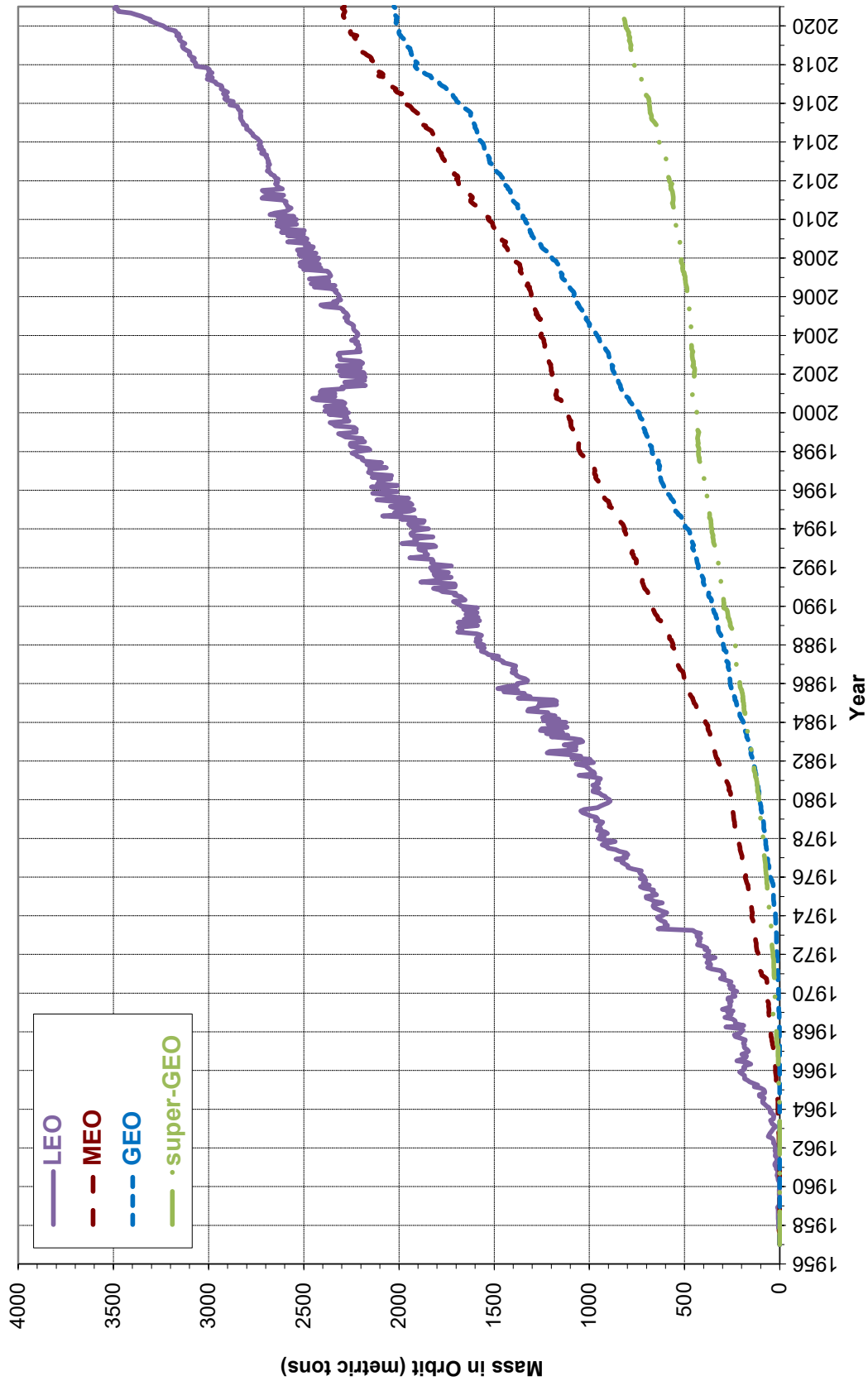
Monthly Effective Mass of Objects in Earth Orbit by Orbital Regime cataloged by the U.S. Space Surveillance Network (SSN), except those with SSN numbers of 80,000 and greater. This chart displays the mass of all objects in Earth orbit officially cataloged by the U.S. Space Surveillance Network. Low Earth orbit (LEO) includes resident space objects (RSOs) with altitudes within or crossing below 2,000 km; middle Earth orbit (MEO) RSOs with altitudes within or crossing the range from 2,000 km to 35,586 km; geosynchronous orbit (GEO) RSOs with altitudes within or crossing the range from 35,586 km to 35,986 km; and the remainder with altitudes within or crossing the range from 35,986 km to 600,000 km. "Effective" number sums the fraction of each orbit that falls within the specified ranges. Cataloged objects without available orbital elements are excluded.

SATELLITE BOX SCORE

Country/ Organization	Spacecraft*	Spent Rocket Bodies & Other Cataloged Debris	Total
CHINA	472	3848	4320
CIS	1552	5737	7289
ESA	93	59	152
FRANCE	74	511	585
INDIA	102	116	218
JAPAN	199	129	328
USA	3819	5133	8952
OTHER	1267	107	1374
TOTAL	7578	15640	23218

* active and defunct

Visit the NASA

Orbital Debris Program Office Website

www.orbitaldebris.jsc.nasa.gov

Technical Editor
Heather Cowardin, Ph.D.

Managing Editor
Rossina Miller

Correspondence can be sent to:

J.D. Harrington
j.d.harrington@nasa.gov

or to:
Nilufar Ramji
nilufar.ramji@nasa.gov

INTERNATIONAL SPACE MISSIONS

01 March 2021 – 31 May 2021

Intl.* Designator	Spacecraft	Country/ Organization	Perigee Alt. (KM)	Apogee Alt. (KM)	Incli. (DEG)	Addnl. SC	Earth Orbital R/B	Other Cat. Debris
1998-067	ISS dispensed payloads	Various	407	410	51.6	9	0	1
2021-017A	STARLINK-2068	US	546	548	53.1	59	1	4
2021-018A	STARLINK-2257	US	547	547	53.1	59	0	4
2021-019A	SHIYAN 9 (SY-9)	PRC	470	35835	19.8	0	1	0
2021-20A	YAOGAN-31 K	PRC	1078	1102	63.4	0	1	2
2021-20C	YAOGAN-31 L	PRC	1078	1102	63.4			
2021-20D	YAOGAN-31 M	PRC	1078	1102	63.4			
2021-21A	STARLINK-2258	US	546	548	53.1	59	0	4
2021-22A	CAS500-1	SKOR	493	510	97.4	36	?	?
2021-23A	VEERY-RL1	US	538	557	45.0	6	1	0
2021-24A	STARLINK-2087	US	547	548	53.1	59	0	4
2021-25A	ONEWEB-0115	UK	1213	1216	87.9	35	0	0
2021-26A	GAOFEN 12 (02)	PRC	628	629	97.9	0	1	0
2021-27A	STARLINK-2048	US	347	353	53.1	59	0	4
2021-28A	SHIYAN 6 03(SY-6 03)	PRC	991	1002	99.5	0	1	0
2021-29A	SOYUZ MS-18	CIS	419	421	51.6	0	1	0
2021-30A	DRAGON ENDEAVOUR 2	US	419	421	51.6	0	0	0
2021-31A	ONEWEB-0176	UK	1012	1022	87.8	35	0	0
2021-32A	USA 314	US	NO INITIAL ELEMENTS			0	0	0
2021-33A	OBJECT A	PRC	496	510	97.4	8	1	0
2021-34A	PNE03	FR	623	625	97.9	5	0	0
2021-35A	CSS (TIANHE-1)	PRC	373	386	41.5	0	1	0
2021-36A	STARLINK-2567	US	348	351	53.1	59	0	4
2021-37A	YAOGAN-34	PRC	1079	1101	63.4	0	1	0
2021-38A	STARLINK-2613	US	546	548	53.1	59	0	4
2021-039A	YAOGAN-30 X	PRC	595	601	35.0	0	1	0
2021-039B	YAOGAN-30 Y	PRC	594	602	35.0			
2021-039C	YAOGAN-30 Z	PRC	596	600	35.0			
2021-039D	TIANQI-12	PRC	589	598	35.0			
2021-40A	STARLINK-2461	US	546	548	53.1	59	0	4
2021-41A	STARLINK-2063	US	546	549	53.1	53	0	5
2021-042A	SBIRS GEO 5 (USA 315)	US	35696	35716	7.9	0	0	0
2021-042B	TDO 3 SPACECRAFT	US	174	4199	26.2			
2021-042C	TDO 4 SPACECRAFT	US	182	4175	26.2			
2021-43A	HAIYANG 2D	PRC	946	958	66.0	0	1	3
2021-44A	STARLINK-2758	US	546	548	53.1	59	0	4
2021-45A	ONEWEB-0211	UK	747	760	87.6	35	0	0
2021-46A	TIANZHOU 2	PRC	373	386	41.5	0	1	3

* Intl. = International; SC = Spacecraft; Alt. = Altitude; Incli. = Inclination; Addnl. = Additional; R/B = Rocket Bodies; Cat. = Cataloged
Notes:
1. Orbital elements are as of data cut-off date 3 July
2. Additional spacecraft on a single launch may have different orbital elements.

The NASA Orbital Debris Photo Gallery has added high resolution, computer-generated images of objects in Earth orbit that are currently being tracked. They may be downloaded. Full instructions are at the webpage:

https://orbitaldebris.jsc.nasa.gov/photo-gallery/